Received: 13 July 2021 | Revised: 16 September 2021 | Accepted: 21 September 2021

DOI: 10.1002/ppap.202100107

RESEARCH ARTICLE

PLASMA PROCESSES AND POLYMERS

Effect of dielectric parameters on the transformation of operation mode and the energy cost of nitrogen fixation of surface microdischarge in air

Chen Lu | **Xingyu Chen** | **Yuqi Wang** | **Yu Zhu** | **Zhenping Zou** | **Zilan Xiong**

State Key Laboratory of Advanced Electromagnetic Engineering and Technology, Huazhong University of Science and Technology, Wuhan, Hubei, China

Correspondence
Zilan Xiong, State Key Laboratory of Advanced Electromagnetic Engineering and Technology, Huazhong University of Science and Technology, Wuhan, 430074 Hubei, China.
Email: zilanxiong@hust.edu.cn

Funding information
National Natural Science Foundation of China, Grant/Award Numbers: 51907076, 52177145

Abstract

In this study, we examine the effect of dielectric parameters (permittivity of the dielectric sheet ε_d and thickness of the dielectric sheet d_d) on the operational mode transformation and energy cost of nitrogen fixation in surface microdischarge (SMD). Three dielectric materials with different thicknesses were used. It was found that d_d has a negative correlation with the power consumption, while a larger ε_d could effectively lower the applied voltage for mode transformation and decrease the energy cost. The trend of energy cost has the shape of a checkmark symbol (√), and the lowest energy cost in this investigation was 489.07 GJ/tN. Increasing ε_d and reducing d_d could further decrease the energy cost in SMD. Finally, the mechanism was briefly discussed.

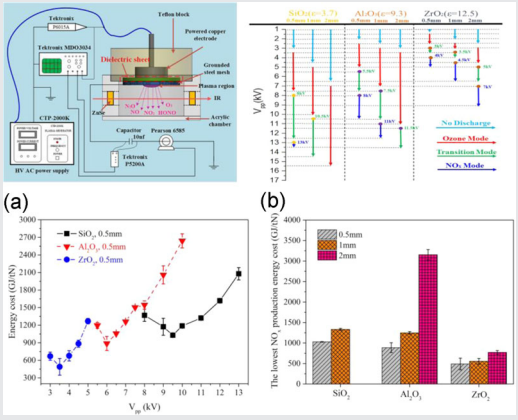

KEYWORDS
dielectric parameters, energy cost, mode transformation, nitrogen fixation, surface microdischarge

1 | INTRODUCTION

Atmospheric-pressure nonequilibrium plasma plays an important role in many fields, such as sterilization and disinfection,[1] biomedicine,[2] environmental protection,[3] material processing,[4] and agriculture,[5] and in the food industry.[6] A large number of atmospheric pressure plasma devices have been developed and modified for different applications, such as dielectric barrier discharge (DBD),[7,8] pin-to-plane discharge,[9,10], and plasma jet.[11,12] Surface microdischarge (SMD) is a type of DBD. A typical SMD source usually consists of a powered electrode, a dielectric sheet, and a grounded mesh electrode. The dielectric sheet is sandwiched between the

powered electrode and the grounded mesh electrode. When used for treatment, the processing object is generally located some millimeters to centimeters below the grounded mesh electrode.

The discharge form of SMD is simple, and the discharge can work directly in ambient air without a noble gas. SMD has been reported to have different operation modes according to the dominant gas-phase products, including ozone, transition, and NO_x modes.[13–17] Under certain conditions, the three operation modes could be transformed, which has been reported to be mainly determined by the power density.[13,18,19] When the discharge power density is low, SMD works in the ozone mode with O_3 as the main gas-phase production; when the power increases to a certain level, the gas-phase production includes both O_3 and NO_x, and the SMD works in transition mode. If the power density continues to increase, NO_x will dominate the gas-phase products without O_3; in this case, we say that the SMD works in the NO_x mode in which the main products contain N_2O, NO, NO_2, HONO, and HNO_3. For all the descriptions in this paper, the terms "mode," "operation mode," "mode transformation," and "transition mode" are all related to the content above.

In addition to the features of mode transformation, SMD also has the advantages of low processing temperature, abundant chemical reaction, and numerous active particles, and has great potential for onychomycosis treatment,[20] material modification,[21] and liquid treatment.[22] Recently, an increasing number of scholars have examined atmospheric-pressure nonequilibrium plasma for nitrogen fixation. The theoretical limit of the energy consumption of nonequilibrium plasma to fix nitrogen is lower than that of the traditional method (the Haber–Bosch process).[23] Meanwhile, nonequilibrium plasma is smart and easy to operate and can be combined with renewable energy technology, such as wind energy and solar energy, to further reduce the consumption of fossil energy and environmental pollution. It is recognized as one of the possible routes for nitrogen transformations that eliminate or minimize the need for fossil fuels.[24] DBD has been extensively studied as a potential method of nitrogen fixation because of its convenient bulk processing. Patil et al.[25] used a packed DBD reactor without a catalyst for nitrogen fixation, and the corresponding lowest energy cost of NO_x was approximately 3850 GJ/tN. Han et al.[26] studied the influence of frequency on nitrogen fixation of a DBD with a single quartz dielectric sheet in air, and the results showed that the corresponding lowest energy cost of NO_x was approximately 5434 GJ/tN. Pei et al.[27] applied a DBD device to make NO_x and investigated the effect of mesh material on NO_x production efficiency, and the results showed that the energy cost of NO_x was in the range of 4000–10 000 GJ/tN for different discharge conditions. Compared with other atmospheric-pressure nonequilibrium plasma sources, the energy cost for nitrogen fixation of DBD is too high, which limits its practical application in industry.[28–30] Therefore, effectively reducing the energy cost for nitrogen fixation of DBD is a key issue to be solved at present.

For a typical DBD, the discharge power is related to many factors, including the applied voltage, the dielectric constant of the dielectric sheet, the thickness of the dielectric sheet, gas gap, and working gas.[31–35] Until now, systematic studies on mode transformation in SMD and the energy cost of nitrogen production have been rare. It has been reported that dielectric properties can affect the discharge intensity and homogeneity of a typical DBD.[36–39] Therefore, for a configuration similar to that of DBD, the discharge properties of the SMD may also be affected by the dielectric parameters.

In this study, we focus on the effect of dielectric parameters on the mode transformation and energy cost of nitrogen fixation in an SMD device. Three types of dielectric materials of three different thicknesses were used in this investigation. Fourier-transform infrared (FTIR) was employed to identify the gas-phase products under different applied voltages and with dielectric sheets having different thicknesses and dielectric constants. A mode transformation map was created, and the energy cost of nitrogen fixation was calculated and compared. Finally, the mechanism of the dielectric parameters on the mode transformation and energy cost reduction was analyzed.

2 | EXPERIMENTAL SETUP AND MEASUREMENTS

2.1 | Experimental setup

Figure 1 shows the structure of the SMD device used in this study. The copper electrode was 20 mm in diameter and 14 mm in height, and it was wrapped in Teflon. A stainless steel mesh with a diameter of 50 mm and a cell density of 5×5 cells/cm^2 was used as the ground electrode. A dielectric sheet was attached between the power electrode and the ground electrode. The SMD device was placed on top of a cylindrical acrylic chamber with an inner diameter of 38 mm and a height of 45 mm. The chamber was used to confine the reactive species produced by the SMD device. Two ZnSe windows (13 mm in diameter) were placed on the wall of the cylindrical acrylic chamber to transmit the IR beam to analyze the composition of the gas-phase products generated by the SMD device. The FTIR path length is 50 mm. A high-voltage and high-frequency AC power supply

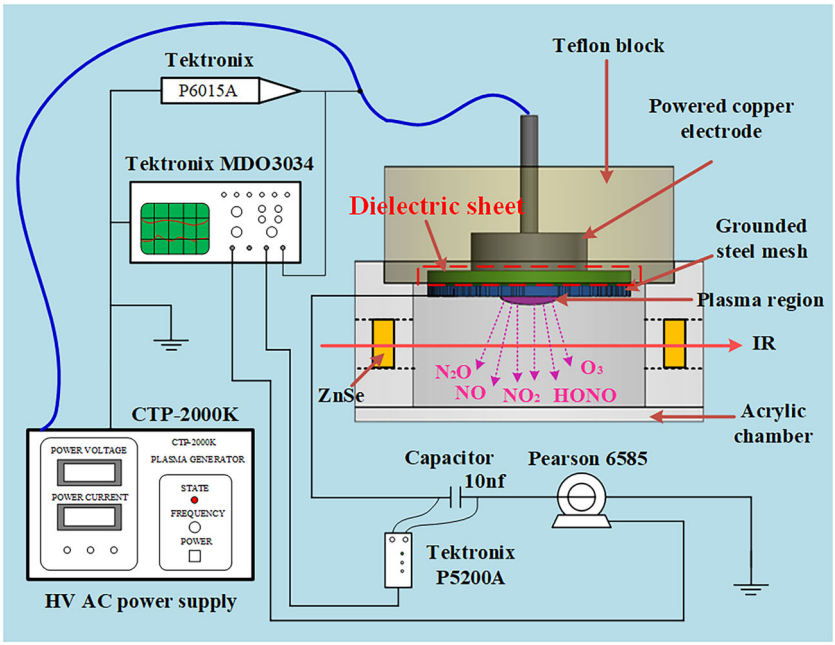

FIGURE 1 Sketch of the surface microdischarge device and the experimental setup

TABLE 1 Three kinds of dielectric sheets used in this study

Dielectric sheet	Dielectric constant	Thickness (mm)
SiO_2	3.7	0.5, 1, 2
Al_2O_3	9.3	0.5, 1, 2
ZrO_2	12.5	0.5, 1, 2

(CTP-2000K; Corona Lab) was used as the power source. The ambient air was used as the working gas for all the experiments with a relative humidity of approximately 75%.

To investigate the effect of the thickness and dielectric constant of the dielectric sheet on the operation mode of the SMD device, three types of dielectric sheets were used in this study, as shown in Table 1.

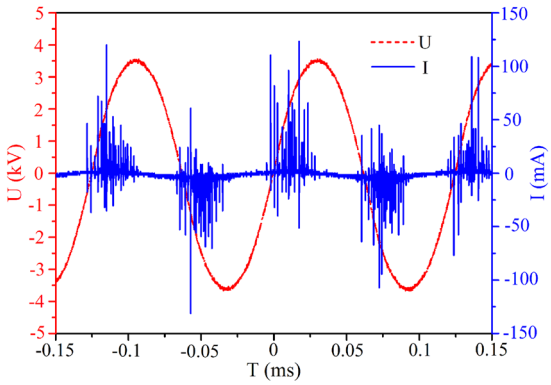

FIGURE 2 Typical *V–I* waveform of the discharge for the surface microdischarge device using 1 mm Al_2O_3 dielectric sheet at an applied voltage V_{p-p} of 7.5 kV

2.2 | Measurements and methods

For all experiments, the frequency of the AC power supply was fixed at 8 kHz. The applied AC voltage amplitude was monitored using a voltage probe (Tektronix P6015A) and an oscilloscope (Tektronix MDO3034). The circuit current was measured using a current probe (Pearson 6585). Figure 2 shows the typical *V–I* waveform of the discharge for the SMD device using a 1 mm Al_2O_3 dielectric sheet with V_{p-p} at 7.5 kV. A 10 nF capacitor was connected in series between the mesh and the ground. The voltage across the capacitor was measured using a differential probe (Tektronix P5200A). The power consumed by the SMD device was obtained using the Lissajous method.

An FTIR spectrometer (VERTEX 70; Bruker) was used as an in situ diagnostics of the chemical composition of the gas produced by the SMD. The wavenumber resolution of the FTIR measurements was set to 4 cm^{-1}, and 16 scans were averaged to create each spectrum. The time resolution of each spectrum was 15 s. The primary gas-phase products generated by the SMD device included N_2O, NO, NO_2, HONO, and O_3. By measuring the standard FTIR spectra of NO_x with known concentrations and comparing the experimental FTIR spectra with the calibrated data, the absolute concentration of NO_x produced by the SMD device was obtained according to Beer's law.

By measuring the discharge power and NO_x concentration of the SMD device, the energy cost of NO_x production was calculated as follows:

$$E_{N_r} = \frac{P \times t}{\frac{V}{24\,L/min} \times c_{NO_x} \times 10^{-6} \times 14\,g/mol} \times 10^{-3}. \quad (1)$$

Here, E_{N_r} is the energy expended per unit of reactive N_r expressed in units of GJ/tN. P is the plasma power consumption (W), t is time (s), V is the volume of the chamber (L), c_{NO_x} is the concentration of NO_x (ppm), 24 L/mol is the molar volume of an ideal gas at 1 atm and 293 K, and 14 g/mol is the molar mass of the N atom. A factor of 10^{-3} arises from the conversion of J/g to GJ/tN. For all energy cost calculations, only the concentrations of NO and NO_2 in gas-phase products were used. At least six samples were used for each test point.

3 | RESULTS

3.1 | Effect of dielectric parameters on power consumption

Figure 3 shows the discharge power consumption of dielectric sheets having different thicknesses and dielectric constants as a function of the applied voltage V_{p-p}. It can be seen that, for a dielectric sheet with the same thickness and the same dielectric constant, the discharge power consumption increases monotonically with an increase in the applied voltage V_{p-p}. Under the same applied voltage V_{p-p}, for the same type of dielectric sheet, that is, the same dielectric constant, the power consumption was negatively correlated with the thickness of the dielectric sheet. For example, for SiO_2, when the applied voltage V_{p-p} is 10 kV, the corresponding discharge power consumption of SiO_2 with thicknesses of 0.5, 1, and 2 mm are 4.17, 1.57, and 0.43 W, respectively. Meanwhile, under the same applied voltage V_{p-p}, for dielectric sheets of the same thickness, the power consumption is positively correlated with the dielectric constant. For instance, for the 1 mm dielectric sheet, when the applied voltage V_{p-p} is 6 kV, the corresponding discharge power consumption of SiO_2, Al_2O_3, and ZrO_2 are 0.19, 0.37, and 5.52 W, respectively.

3.2 | Typical FTIR spectrum and its corresponding NO_x concentration

Figure 4a shows a typical FTIR spectrum of the SMD device with a 1 mm dielectric sheet made of Al_2O_3. It can be seen that the main product of the SMD device at an applied voltage V_{p-p} of 4.5 kV is ozone (1055 cm^{-1}); when the applied voltage V_{p-p} increases to 12 kV, the main gas-phase products of the SMD are nitrogen oxides, including NO at 1900 cm^{-1}, NO_2 at 1630 cm^{-1}, and HONO at 1255 cm^{-1}. For the 1 mm Al_2O_3 dielectric sheet, when the applied voltage V_{p-p} is 12 kV, the time evolution of NO_x concentrations is shown in Figure 4b. The concentration of HONO and HNO_3 was relatively low and nearly had no effect on the energy cost calculation, therefore, the main gas-phase products NO_2 and NO were used. The production rate of NO_x reached up to the highest point of 172.5 ppm/s at 75 s; when the discharge time exceeded 75 s, the growth rate of NO_x concentrations in the SMD chamber began to slow down. Referring to other literature,[27,30] for all the energy cost calculations in this study, the period from the start of the discharge to the discharge time of time point with the highest production rate of NO_x was used. Figure 4c shows the time evolution of NO_x and O_3 concentrations of the 1 mm Al_2O_3 dielectric sheet at an applied voltage V_{p-p} of 8 kV under a transition mode. Under these conditions, ozone was generated first and then disappeared, and when the discharge time exceeded 135 s, no ozone could be detected by FTIR.

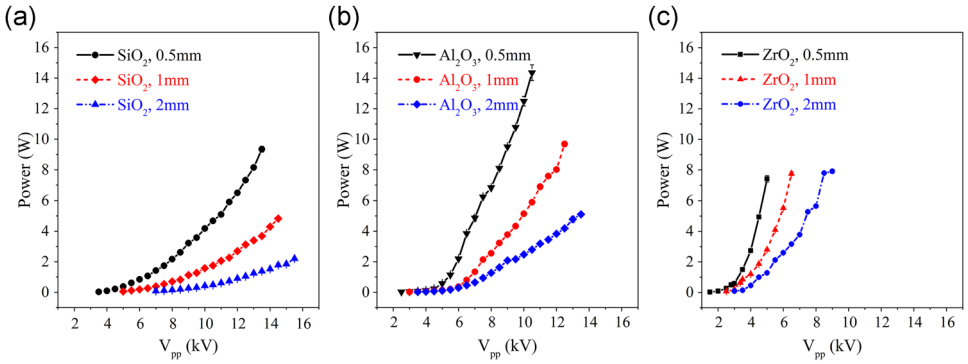

FIGURE 3 Effect of dielectric sheet properties on discharge power consumption. (a) SiO_2; (b) Al_2O_3; (c) ZrO_2

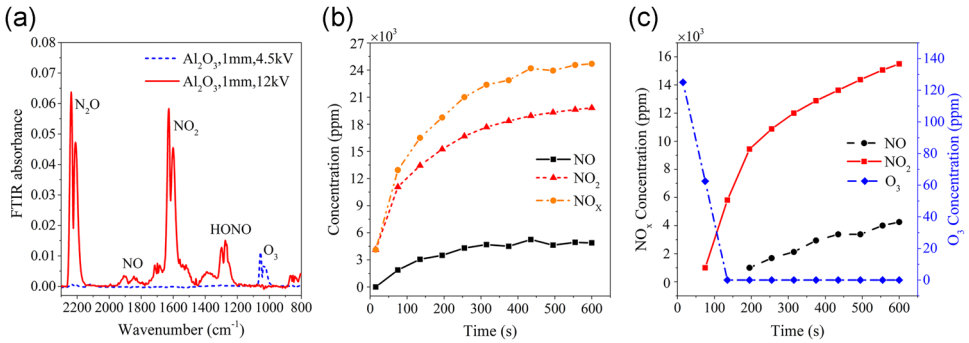

FIGURE 4 (a) Typical Fourier-transform infrared (FTIR) spectrum for the surface microdischarge device with the 1 mm Al_2O_3 dielectric sheet at an applied voltage V_{p-p} of 4.5 and 12 kV, respectively. (b) Measured time-evolution of NO_x concentrations for the 1 mm Al_2O_3 dielectric sheet at an applied voltage V_{p-p} of 12 kV. (c) Measured time-evolution of NO_x and O_3 concentrations of the 1 mm Al_2O_3 dielectric sheet at an applied voltage V_{p-p} of 8 kV

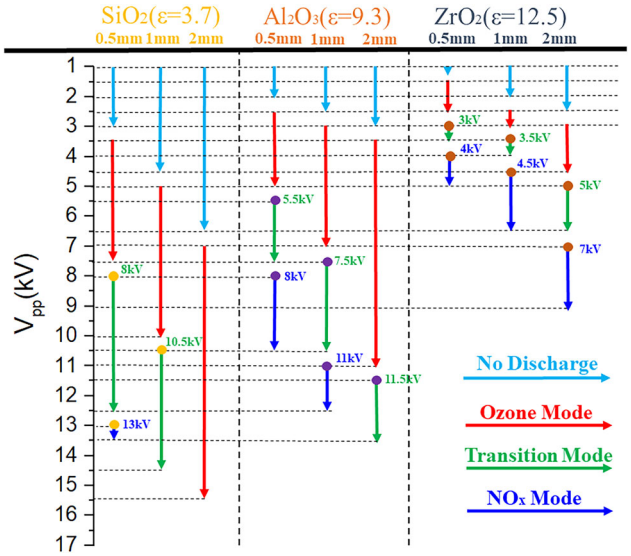

FIGURE 5 Effect of a dielectric sheet on the operation mode of surface microdischarge

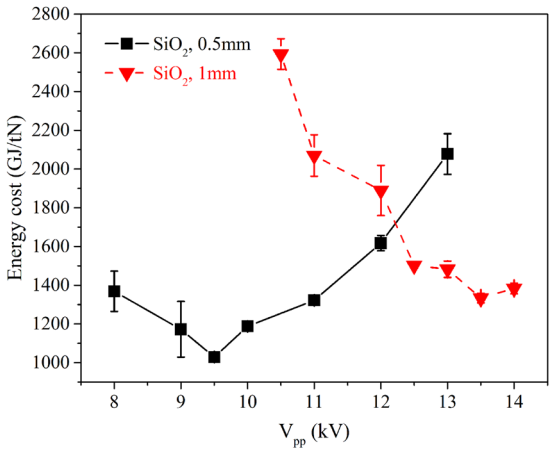

FIGURE 6 Calculated specific energy cost for nitrogen fixation plotted as a function of the applied voltage V_{p-p} at different thicknesses of SiO_2

3.3 | Effect of dielectric parameters on operation modes of SMD

Figure 5 shows the effect of the dielectric parameters on the SMD operation mode. In this paper, we refer to "ozone mode" as the set of conditions in which O_3 is the main product of the SMD device and no NO or NO_2 is presented in the gas phase; "transition mode" is the set of conditions where O_3, NO, and NO_2 can be detected simultaneously during the beginning period of discharge; "NO_x mode" is the set of conditions where NO_x are the main products, and no O_3 can be detected. It can be seen that for the same type of dielectric sheet, that is, when the dielectric constant remains the same, the breakdown voltage and the transfer voltage for different operation modes of the SMD device increase with an increase in the thickness of the dielectric sheet. For dielectric sheets of the same thickness, the breakdown voltage and the transfer voltage of different operational modes of the SMD device decrease with an increase in the dielectric constant. A larger dielectric constant and lesser thickness can effectively reduce the breakdown voltage as well as the mode transfer voltage. In particular, for a ZrO_2 sheet with a thickness of 0.5 mm, the breakdown voltage was reduced to less than 1.5 kV, and at around 3.5 kV, the SMD switched to NO_x mode. However, for SiO_2 with a thickness of 2 mm, no NO or NO_2 was detected in any of the tested voltage ranges.

3.4 | Effect of dielectric parameters on energy cost for nitrogen fixation of SMD

Figure 6 shows the calculated specific energy cost of NO_x production as a function of the applied voltage

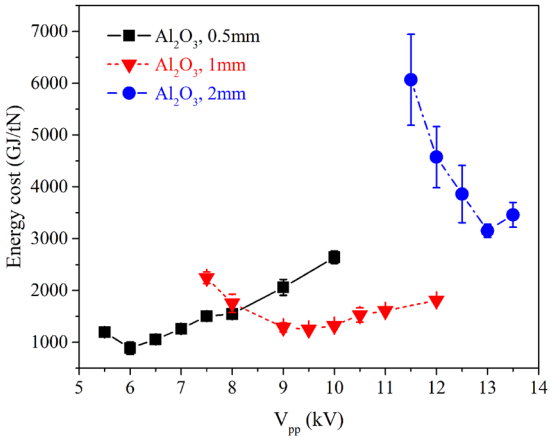

FIGURE 7 Calculated specific energy cost for nitrogen fixation plotted as a function of the applied voltage V_{p-p} at different thicknesses of Al_2O_3

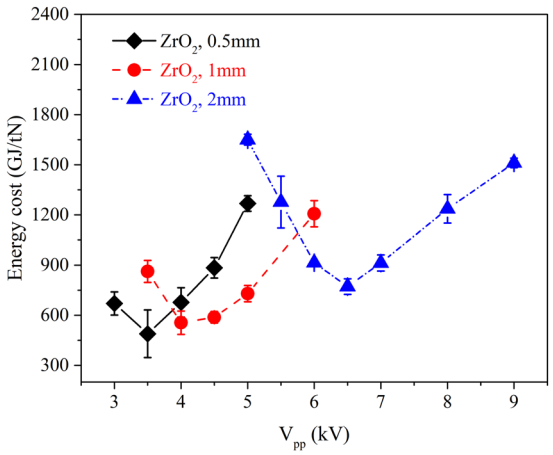

FIGURE 8 Calculated specific energy cost for nitrogen fixation plotted as a function of the applied voltage V_{p-p} at a different thickness of ZrO_2

V_{p-p} with different SiO_2 thicknesses. For SiO_2 with thicknesses of 0.5 and 1 mm, the NO_x production energy cost decreases first and then increases with an increase in the applied voltage V_{p-p}. For the SiO_2 with a thickness of 0.5 mm, when the applied voltage V_{p-p} is 9.5 kV, the lowest NO_x production energy cost is reached at 1029.48 GJ/tN. For the SiO_2 with a thickness of 1 mm, when the applied voltage V_{p-p} is 13.5 kV, the lowest NO_x production energy cost is 1333.46 GJ/tN. It can be concluded that the lowest NO_x production energy cost of the SiO_2 with a thickness of 0.5 mm is less than that of the SiO_2 with a thickness of 1 mm. At the same time, the voltage V_{p-p} applied to the SiO_2 with a thickness of 0.5 mm to reach the lowest NO_x production energy cost is smaller than that applied to the SiO_2 with a thickness of 1 mm. From the mode transformation map, it can be observed that the lowest energy cost point is within the transition mode range.

Figure 7 shows the calculated energy cost of NO_x production as a function of the applied voltage V_{p-p} with different thicknesses of Al_2O_3. The overall trend was similar to that in the SiO_2 group. For Al_2O_3 with thicknesses of 0.5, 1, and 2 mm, the NO_x production energy cost decreases first and then increases with an increase in the applied voltage V_{p-p}. For the Al_2O_3 with a thickness of 0.5 mm, when the applied voltage V_{p-p} is 6 kV, the lowest NO_x production energy cost is reached at 760.03 GJ/tN. For the Al_2O_3 with a thickness of 1 mm, when the applied voltage V_{p-p} is 9.5 kV, the lowest NO_x production energy cost is 1247.55 GJ/tN. For the Al_2O_3 with a thickness of 2 mm, when the applied voltage V_{p-p} is 13 kV, the lowest NO_x production energy cost reaches 3153.65 GJ/tN.

Figure 8 shows the calculated energy cost for nitrogen fixation as a function of the applied voltage V_{p-p} with different thicknesses of ZrO_2. Similar to those in the SiO_2 and Al_2O_3 groups, for ZrO_2 with thicknesses of 0.5, 1, and 2 mm, the energy cost first decreases with the applied voltage V_{p-p} and then increases. For ZrO_2 with a thickness of 0.5 mm, when the applied voltage V_{p-p} is 3.5 kV, the lowest energy cost is reached at 489.07 GJ/tN. For the ZrO_2 with a thickness of 1 mm, when the applied voltage V_{p-p} is 4 kV, the lowest energy cost is at 555.08 GJ/tN. For ZrO_2 with a thickness of 2 mm, when the applied voltage V_{p-p} is 6.5 kV, the lowest energy cost reaches 771.36 GJ/tN.

3.5 | Comparison of energy cost for nitrogen fixation of dielectric sheets with different dielectric parameters

For a better insight into the dielectric parameters of the energy cost of nitrogen fixation by SMD, we further compared the energy cost with different dielectric constants at a thickness of 0.5 mm, as shown in Figure 9a. It can be seen that increasing the dielectric constant can significantly reduce the energy cost for nitrogen fixation. In addition, for SiO_2, Al_2O_3, and ZrO_2 with thicknesses of 1 or 2 mm, similar results are obtained. For SiO_2, Al_2O_3, and ZrO_2 with a thickness of 0.5 mm, the lowest NO_x production energy costs are 1029.48, 760.03, and 489.07 GJ/tN, respectively. Figure 9b shows a comparison of the lowest NO_x production energy costs of dielectric sheets with different thicknesses and different dielectric constants. It can be concluded that, under the same dielectric constant, the lowest NO_x production

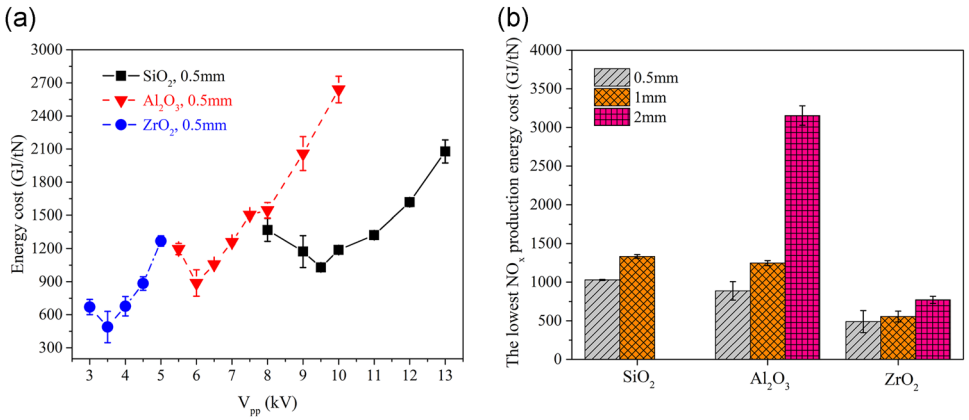

FIGURE 9 (a) Calculated specific energy cost of NO_x production plotted as a function of the applied voltage V_{p-p} at different dielectric constants of the dielectric sheet. The thickness of the three kinds of the dielectric sheet was fixed at 0.5 mm. (b) Comparison of the lowest NO_x production energy cost of the dielectric sheets with different thicknesses and different dielectric constants

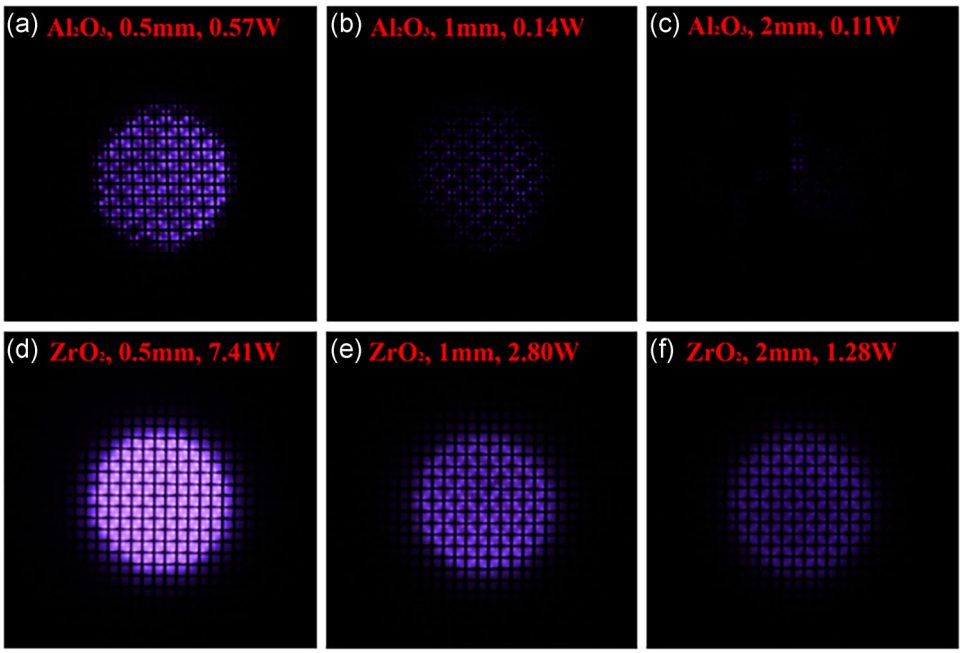

FIGURE 10 Discharge images of the surface microdischarge device corresponding to Al_2O_3 and ZrO_2 dielectric sheets with thicknesses of 0.5, 1, and 2 mm. The applied voltage V_{p-p} is 5 kV

energy cost increases as the thickness of the dielectric sheet increases. Under the same thickness, the lowest NO_x production energy cost decreases with an increase in the dielectric constant.

4 | DISCUSSION

The existing literature on the mode transfer of SMD mainly focuses on power density.[13,18,19] In this study, we found the same trend for a fixed SMD device with a fixed dielectric sheet. However, a single dependence on the power density is not practical when dielectric sheet properties change. We also found that the dielectric parameters have a significant influence on the mode transfer; a lower applied voltage and power density for mode transfer were found with a larger dielectric constant, while a higher applied voltage and power density were needed with a thicker dielectric sheet.

Researchers have found that the dielectric parameters can affect the discharge in typical DBD.[36–39] In our investigation, we found results similar to those of SMD. Figure 10 shows the discharge images of the SMD device corresponding to Al_2O_3 and ZrO_2 dielectric sheets with

thicknesses of 0.5, 1, and 2 mm when the applied voltage V_{p-p} is 5 kV. It clearly shows that the dielectric properties have an obvious effect on the discharge of SMD: the dielectric constant is positively related to the discharge intensity, and the thickness of the dielectric sheet is negatively correlated to the discharge density.

The dielectric constant and thickness of the dielectric sheet have a significant influence on the voltage across the gas gap of the DBD, and the discharge properties are directly related to the voltage across the gas gap.[40,41] An SMD is actually a type of DBD; the equivalent electric circuit of an SMD is comparable to the classic equivalent electric circuit of a DBD. To analyze the effect of dielectric parameters on the gas gap voltage, an equivalent electric circuit was built. Figure 11a,b shows the electrode configurations of a typical DBD and SMD, respectively. Unlike the typical DBD, the gas gap between the mesh electrode and dielectric sheet in the SMD device is irregular. Figure 11c shows the corresponding equivalent electric circuit. In this electric circuit, C_g and C_d represent the equivalent capacitances of the gap and dielectric layer, respectively. $U_a(t)$ is the applied voltage, $U_d(t)$ is the voltage across the dielectric barrier, and $U_g(t)$ is the voltage across the gas gap; I_a is the total external circuit current; I is the discharge current in the gas gap, and I is a function of $U_g(t)$.

According to the equivalent electric circuit shown in Figure 11c, the following equations can be obtained using Kirchhoff's laws[42-44]:

$$C_d = \varepsilon_0 \varepsilon_d \frac{S_d}{d_d}, \tag{2}$$

$$C_g = \varepsilon_0 \varepsilon_g \frac{S_g}{d_g}, \tag{3}$$

$$U_a(t) = U_d(t) + U_g(t), \tag{4}$$

$$U_d(t) = \frac{1}{C_d} \int_0^t I_a(\tau) d\tau, \tag{5}$$

$$V_m = 3000 \times d_g + 2 \times d_d \times \frac{3000}{\varepsilon_d}, \tag{6}$$

where ε_0 is the permittivity of vacuum, ε_d is the permittivity of the dielectric barrier, ε_g is the permittivity of the gas, d_d is the thickness of the dielectric barrier, d_g is the gas gap distance, S_d is the area of the dielectric barrier, and S_g is the area of the electrodes. From Equation (2), C_d is proportional to ε_d and inversely proportional to d_d. V_m is the minimum external voltage at which ignition occurs. From Equation (5), U_d is inversely proportional to C_d. It should be noted that for the SMD device used in this study, d_g, S_g, and S_d remain constant, and therefore, C_g remains constant.

The dielectric parameters ε_d and S_d mainly affect the capacitance of the dielectric sheet C_d, as well as the minimum external breaking down voltage V_m. (1) Under smaller d_d and larger ε_d, the discharge is much easier to ignite; (2) under the same conditions, for the same U_a, when ε_d remains constant if d_d is small, C_d is large. The voltage on the dielectric sheet U_d is small, increasing the voltage as the gas gap U_g becomes higher, causing the discharge to become more intense; (3) under the same conditions, for the same U_a, when d_d remains constant, if ε_d is large, C_d is large. Thus, if U_d is small, U_g becomes large and causes the discharge to become more intense. It can be concluded that, when ε_d is the same, U_g increases with a decrease in d_d, so the transfer voltage of different operational modes of SMD decreases with the decrease in d_d. When d_d is the same, U_g increases with an increase in ε_d, so the transfer voltage of different operational modes of SMD decreases with the increase in ε_d. These conclusions were consistent with the experimental results of this study.

Compared with other nitrogen fixation methods for plasma with different configurations, SMD more easily achieves large-scale nitrogen oxide production and stable operation. Our study also found that the dielectric parameters had a significant effect on the energy cost for nitrogen fixation in SMD. With similar dielectric property conditions,

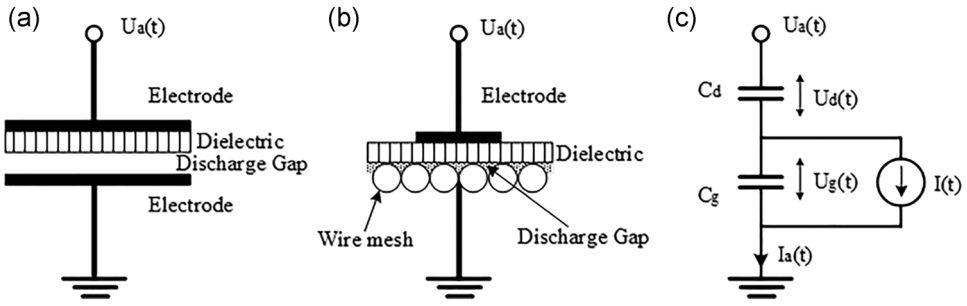

FIGURE 11 (a) Typical dielectric barrier discharge electrode configuration. (b) Sketch of the surface microdischarge. (c) Corresponding equivalent electric circuit

for example, Al_2O_3 with a thickness of 1–2 mm, the energy cost is close to that of Pei et al.[27] With a relatively higher dielectric constant and thinner dielectric sheet, the lowest specific energy cost in this study is reduced to 489.07 GJ/tN, which is at least eight times lower than the NO_x production energy cost of DBD reported in other references.[25–27] Based on the results of this study, we can further optimize the discharge parameters of SMD, such as using a dielectric sheet with a larger dielectric constant and a smaller thickness to further reduce the transfer voltage of different operational modes of SMD and obtain lower NO_x production energy costs.

For SiO_2 with thicknesses of 0.5 or 1 mm, and Al_2O_3 and ZrO_2 with thicknesses of 0.5, 1, or 2 mm, after entering into transition mode, the trend of energy cost for NO_x fixation takes the shape of a checkmark symbol ($\surd$), and the lowest energy cost points for NO_x production are all within the transition mode. This trend is similar to that observed in a DC pin–pin discharge when the applied voltage is increased.[30] One possible reason for the results is that when SMD works in the transition mode, the gas temperature and the temperature of the wire ground electrode and around the electrode increases with the power consumption, and the increase in temperature has a substantial promotion; effect on the reaction rate constant and reaction rate, making the growth rate of NO_x production faster than that of discharge power consumption; thus, the energy cost for nitrogen fixation decreases with the increase in applied voltage. When the applied voltage further increases, the benefit of the NO_x production rate and the energy cost brought by temperature becomes weaker, while the proportion of energy waste by Joule heating further increases, increasing the energy cost for nitrogen fixation. To further understand the reason for this finding, more work needs to be conducted to gain insight into the transition mode.

5 | CONCLUSION

The systematic study of mode transformation and nitrogen fixation of SMD is of great importance for practical applications. In this study, the effect of applied voltage V_{p-p}, the thickness of the dielectric sheet, and the dielectric constant of the dielectric sheet on the discharge power consumption, operation mode, and energy cost of nitrogen fixation of SMD were studied. The dielectric parameters could significantly affect the breakdown voltage, mode transfer voltage, and energy cost for nitrogen fixation in SMD. This was mainly caused by changing the equivalent capacitance of the dielectric sheet through the dielectric constant and thickness, which finally affects the gas gap voltage across the discharge area. The lowest energy cost was 489.07 GJ/tN in this investigation using ZrO_2 with a thickness of 0.5 mm. Reducing the thickness of the dielectric sheet and increasing the dielectric constant could further reduce the mode transfer voltage and lower the energy cost for nitrogen fixation in SMD. All of the lowest energy cost points were within the transition mode region, which may be caused by the competition between the reaction rate constant and the reaction rate promotion induced by the temperature and energy waste of Joule heating, which requires further study.

ACKNOWLEDGMENTS

The authors are grateful for financial support from the National Natural Science Foundation of China (No. 51907076 and No. 52177145).

DATA AVAILABILITY STATEMENT

The data that supports the findings of this study are available within the article.

ORCID

Zilan Xiong https://orcid.org/0000-0003-1095-3959

REFERENCES

[1] W. Xi, W. Wang, Z. Liu, Z. Wang, L. Guo, X. Wang, M. Rong, D. Liu, *Plasma Sources Sci. Technol.* **2020**, *29*, 095013.
[2] S. Zhao, R. Han, Y. Li, C. Lu, X. Chen, Z. Xiong, X. Mao, *J. Appl. Phys.* **2019**, *125*, 163301.
[3] L. Schückel, J.-L. Gembus, N. Peters, F. Kogelheide, R. T. Nguyen-Smith, A. R. Gibson, J. Schulze, M. Muhler, P. Awakowicz, *Plasma Sources Sci. Technol.* **2020**, *29*, 114003.
[4] K. G. Kostov, T. M. C. Nishime, A. H. R. Castro, A. Toth, L. R. O. Hein, *Appl. Surf. Sci.* **2014**, *314*, 367.
[5] Y. Zhu, Z. Xiong, M. Li, X. Chen, C. Lu, Z. Zou, *Plasma Processes Polym.* **2021**, *18*, e2000223.
[6] X. Liao, Y. Su, D. Liu, S. Chen, Y. Hu, X. Ye, J. Wang, T. Ding, *Food Control* **2018**, *94*, 307.
[7] D. Mei, X. Zhu, Y. He, J. D. Yan, X. Tu, *Plasma Sources Sci. Technol.* **2015**, *24*, 015011.
[8] Q. Ye, Y. Wu, X. Li, T. Chen, G. Shao, *Plasma Sources Sci. Technol.* **2012**, *21*, 065008.
[9] K. Yanallah, F. Pontiga, *Plasma Sources Sci. Technol.* **2012**, *21*, 045007.
[10] J. Khun, V. Scholtz, P. Hozák, P. Fitl, J. Julák, *Plasma Sources Sci. Technol.* **2018**, *27*, 065002.
[11] X. Yan, Z. Xiong, F. Zou, S. Zhao, X. Lu, G. Yang, G. He, K. Ostrikov, *Plasma Processes Polym.* **2012**, *9*, 59.
[12] I. V. Schweigert, A. L. Alexandrov, D. E. Zakrevsky, *Plasma Sources Sci. Technol.* **2020**, *29*, 12LT02.
[13] M. J. Pavlovich, D. S. Clark, D. B. Graves, *Plasma Sources Sci. Technol.* **2014**, *23*, 065036.
[14] T. Shimizu, Y. Sakiyama, D. B. Graves, J. L. Zimmermann, G. E. Morfill, *New J. Phys.* **2012**, *14*, 103028.
[15] Y. Sakiyama, D. B. Graves, H.-W. Chang, T. Shimizu, G. E. Morfill, *J. Phys. D: Appl. Phys.* **2012**, *45*, 425201.
[16] T. Maisch, T. Shimizu, G. Isbary, J. Heinlin, S. Karrer, T. G. Klämpfl, Y.-F. Li, G. E. Morfill, J. L. Zimmermann, *Appl. Environ. Microbiol.* **2012**, *78*, 4242.

[17] J. L. Zimmermann, K. Dumler, T. Shimizu, G. E. Morfill, A. Wolf, V. Boxhammer, J. Schlegel, B. Gansbacher, M. Anton, *J. Phys. D: Appl. Phys.* **2011**, *44*, 505201.
[18] M. J. Pavlovich, H.-W. Chang, Y. Sakiyama, D. S. Clark, D. B. Graves, *J. Phys. D: Appl. Phys.* **2013**, *46*, 145202.
[19] M. J. Pavlovich, Y. Sakiyama, D. S. Clark, D. B. Graves, *Plasma Processes Polym.* **2013**, *10*, 1051.
[20] Z. Xiong, R. Huang, Y. Zhu, K. Luo, M. Li, Z. Zou, R. Han, *Plasma Processes Polym.* **2021**, *18*, e2000204.
[21] C. Lu, J. Dai, N. Dong, Y. Zhu, Z. Xiong, *Plasma Processes Polym.* **2020**, *17*, e2000100.
[22] D. Liu, Z. Liu, C. Chen, A. Yang, D. Li, M. Z. Rong, H. Chen, M. G. Kong, *Sci. Rep.* **2016**, *6*, 23737.
[23] W. Wang, B. Patil, S. Heijkers, V. Hessel, A. Bogaerts, *ChemSusChem* **2017**, *10*, 2145.
[24] S. Chen, M. Z. Mo, Z. Chen, R. K. Li, M. Dunning, B. B. L. Witte, J. K. Baldwin, L. B. Fletcher, J. B. Kim, A. Ng, R. Redmer, A. H. Reid, P. Shekhar, X. Z. Shen, M. Shen, K. Sokolowski-Tinten, Y. Y. Tsui, Y. Q. Wang, Q. Zheng, X. J. Wang, S. H. Glenzer, *Science* **2018**, *360*, 873.
[25] B. S. Patil, N. Cherkasov, J. Lang, A. O. Ibhadon, V. Hessel, Q. Wang, *Appl. Catal., B* **2016**, *194*, 123.
[26] Y. Han, S. Wen, H. Tang, X. Wang, C. Zhong, *Plasma Sci. Technol.* **2018**, *20*, 014001.
[27] X. Pei, D. Gidon, Y.-J. Yang, Z. Xiong, D. B. Graves, *Chem. Eng. J.* **2019**, *362*, 217.
[28] X. Hao, A. M. Mattson, C. M. Edelblute, M. A. Malik, L. C. Heller, J. F. Kolb, *Plasma Processes Polym.* **2014**, *11*, 1044.
[29] M. Janda, V. Martiš ovit š, K. Hensel, Z. Machala, *Plasma Processes Polym.* **2016**, *36*, 767.
[30] X. Pei, D. Gidon, D. B. Graves, *J. Phys. D: Appl. Phys.* **2020**, *53*, 044002.
[31] J. Kriegseis, B. Möller, S. Grundmann, C. Tropea, *J. Electrostat.* **2011**, *69*, 302.
[32] X. Zhang, B. J. Lee, H. G. Im, M. S. Cha, *IEEE Trans. Plasma Sci.* **2016**, *44*, 2288.
[33] J. Pons, E. Moreau, G. Touchard, *J. Phys. D: Appl. Phys.* **2005**, *38*, 3635.
[34] L. Dong, W. Fan, Y. He, F. Liu, *IEEE Trans. Plasma Sci.* **2008**, *36*, 1356.
[35] S. Li, T. V. Raak, F. Gallucci, *J. Phys. D: Appl. Phys.* **2020**, *53*, 014008.
[36] R. Li, Q. Tang, S. Yin, T. Sato, *Appl. Phys. Lett.* **2007**, *90*, 131502.
[37] N. Osawa, Y. Yoshioka, *IEEE Trans. Plasma Sci.* **2012**, *40*, 2.
[38] Z. Fang, Y. Qiu, C. Zhang, E. Kuffel, *J. Phys. D: Appl. Phys.* **2007**, *40*, 1401.
[39] Z. Fang, J. Lin, X. Xie, Y. Qiu, E. Kuffel, *J. Phys. D: Appl. Phys.* **2009**, *42*, 085203.
[40] U. N. Pal, P. Gulati, N. Kumar, M. Kumar, M. S. Tyagi, B. L. Meena, A. K. Sharma, R. Prakash, *IEEE Trans. Plasma Sci.* **2011**, *39*, 1475.
[41] A. Eid, K. Takashima, A. Mizuno, *IEEE Trans. Ind. Appl.* **2014**, *50*, 4221.
[42] S. Liu, M. Neiger, *J. Phys. D: Appl. Phys.* **2003**, *36*, 3144.
[43] Z. Fang, S. Ji, J. Pan, T. Shao, C. Zhang, *IEEE Trans. Plasma Sci.* **2012**, *40*, 883.
[44] C. Zhang, T. Shao, Y. Yu, Z. Niu, P. Yan, Y. X. Zhou, *J. Electrostat.* **2010**, *68*, 445.

How to cite this article: C. Lu, X. Chen, Y. Wang, Y. Zhu, Z. Zou, Z. Xiong, *Plasma Processes Polym.* **2021**, e2100107.
https://doi.org/10.1002/ppap.202100107